Hindawi
International Journal of Chemical Engineering
Volume 2022, Article ID 9217918, 10 pages
https://doi.org/10.1155/2022/9217918

Research Article

Simulation Research of the *n*-Butanol Proportion Influence on HCCI Combustion of Free-Piston Diesel Engine Generators

Chunhui Liu and Hao Zheng

College of Mechanical Engineering, Anhui Science and Technology University, Chuzhou 233100, China

Correspondence should be addressed to Chunhui Liu; liuch@ahstu.edu.cn

Received 14 April 2022; Accepted 9 May 2022; Published 2 June 2022

Academic Editor: Ayon Tarafdar

For researching the influence of *n*-butanol proportion in diesel fuel on homogeneous charge compression ignition (HCCI) combustion of the free-piston diesel engine generator (FPDEG), a three-dimensional (3D) moving mesh computational fluid dynamics (CFD) simulation model of a FPDEG prototype was developed. A detailed chemical reaction mechanism of diesel fuel was selected as the HCCI combustion mechanism and coupled in the established HCCI combustion simulation model of the FPDEG prototype. The validity of the established HCCI combustion simulation model is proved by comparing the simulation and experimental pressure curves under the condition of pure diesel fuel. The simulation results of different *n*-butanol proportions in diesel fuel showed that as the *n*-butanol proportion increased from 0 to 60%, the maximum heat release rate decreased to 59.6 J/deg, the calculated indicated thermal efficiency augmented to 4.6%, the calculated indicated mean effective pressure increased to 0.057 MPa, and the final NO_x and CO content decreased to 0.239 and 0.57 g/kg fuel, respectively, but the final soot content increased to 0.000562 g/kg fuel. Therefore, the *n*-butanol proportion of diesel fuel played a vital role in combustion and emission progress of the FPDEG.

1. Introduction

Nowadays, the engine with internal combustion has become the most extensive technology and spends most of the oil [1, 2]. Nonetheless, its low efficiency and high emission need to be solved urgently under the increasingly strict energy-saving and environmental protection requirements. Therefore, HCCI combustion, the most potential technology, was explored to protect the environment and improve the efficiency.

HCCI combustion can achieve about 20% efficiency improvement and near-zero emission of NO_x under specific conditions [3–5]. However, conventional HCCI engines lack effective means to precisely control how fast the fuel evaporates, which makes the practical HCCI combustion engines impossible to use in the full-operation range demanded by the automotive power system [6–9]. Therefore, to make full use of HCCI combustion, a new engine type different from the traditional engine is required to adjust to the HCCI mode [10–12].

Obviously, the structure of the free-piston engine (FPE) is simpler than that of the engine in wide use because FPE eliminates the crank-connecting rod. The FPE can be applied in many areas, such as electric generator. Now, the free-piston engine generator (FPEG) has become increasingly significant [13–15]. The compression ratio of the FPEG is variable, which is a perfect match for HCCI combustion, so the study of the FPDEG HCCI combustion will have a strong operability.

In the 1990s, with the rapid development of computer, electronic, and hydraulic technology, many researchers began to study the FPEG. Atkinson [16] used the law of thermodynamics to simulate the scavenging, compression, and combustion processes of a prototype and analyzed the effects of piston mass, ignition, and combustion heat release on the motion characteristics of the prototype. Cawthorne [17] established the model of the integrated engine and the linear motor and studied their matching problem through the numerical analysis of the model. Plsek [18] established

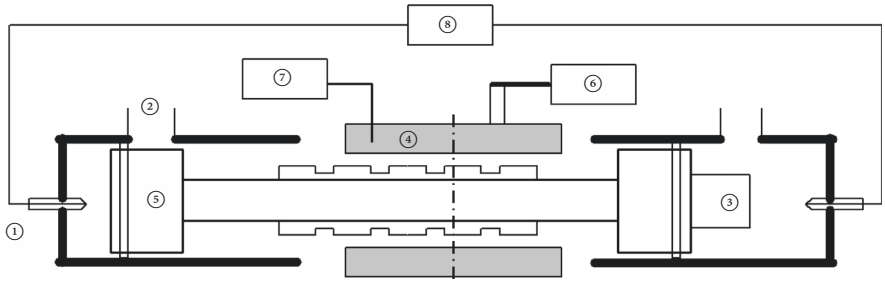

Figure 1: The structural type of the FPDEG prototype. (1) Fuel injector; (2) exhaust; (3) scavenge; (4) linear motor; (5) free piston; (6) electromagnetic load; (7) motor mode conversion controller; (8) fuel injection controller.

the mathematical models of dynamics, thermodynamics, and power electronic dynamics for the designed FPEG system by using Matlab/Simulink and DSPACE software, and on this basis, the closed-loop control strategy of the current and position was studied. The Huang research group [19] put up an experimental platform and analyzed the dynamics and system performance of the FPEG by numerical simulation. The Zuo research group [20, 21] built a FPEG prototype and studied its operation, including nonlinear dynamics, performance analysis, control strategy, and performance test. Many multidimensional CFD models have been developed to investigate the comprehensive performance of the FPEG prototypes, for example, the models of Newcastle University [22, 23], the Chalmers University of Technology [24], and the Beijing Institute of Technology [20, 21]. These models were developed based on the corresponding FPEG prototypes, which guaranteed their high accuracy. However, most of the coupled reaction mechanisms in the above models were one-step or several-step reactions reduced mechanisms. Because the key components and reactions were ignored in the reduced mechanisms, the combustion process simulation accuracy was not high and the applicable working condition range was smaller.

Nowadays, the air pollution problem is drawing more attention. In order to reduce air pollution, the clean fuel is essential in the internal combustion engines. Butanol is a biofuel originating from the organic material fermentation and has more advantages than methanol and ethanol, such as higher heating value, lower volatility, better cold start ignition performance, and water pollution tolerance. Therefore, it has been widely applied as a clean fuel or additive in all kinds of engines [25–29].

In this paper, the opposed-piston two-stroke FPDEG, the same as the prototype of the Beijing Institute of Technology, was selected as the research object and its simulation model coupling a relatively detailed fuel mechanism was operated to gain the influence of the *n*-butanol proportion on HCCI combustion.

2. The Simulation Model of FPDEG

Figure 1 shows the structural type of the FPDEG prototype. The working process of the prototype includes two stages: starting stage and operating stage. At the starting stage, the linear motor as a motor provides the starting energy for the system and the mixture in the two cylinders is compressed

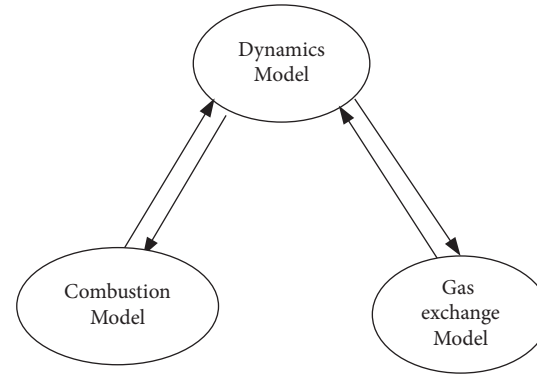

Figure 2: The iterative calculation schematic diagram.

alternately; in the meantime, the fuel injection system injects diesel under the control signal. At the operating stage, the linear motor works no longer as a motor, but as a generator through cutting the magnetic field of the linear motor to produce electromotive force. At this point, the right and left cylinders alternately complete the ignition and combustion progress and the explosion pressure generated from one cylinder will push the actuator to compress the opposite cylinder.

The motion characteristics of the FPDEG are determined by the pressure, friction, and electromagnetic resistance in two cylinders. Making a contrast between the FPDEG and the traditional diesel engine, the FPDEG's piston displacement, velocity, and acceleration curves have significant changes. Hence, the CFD modeling of the FPDEG is impossible to follow the CFD modeling method of the traditional diesel engine completely.

Figure 2 shows the iterative calculation schematic diagram [30]. Through the dynamic modeling and the iterative calculation of the coupled gas exchange and combustion, the displacement curve of the FPDEG can be obtained. Then, the 3D CFD model of the FPDEG can be established using the calculated piston motion law of the FPDEG. In order to improve the calculation accuracy, the displacement curve should be made into a readable data file to find the position of the piston in the cylinder.

The prototype was completed by motor selection, engine design, subsystem design, processing, assembly, debugging, and adjustment. HCCI combustion can be achieved by early in-cylinder injection. The detailed piston displacement curve

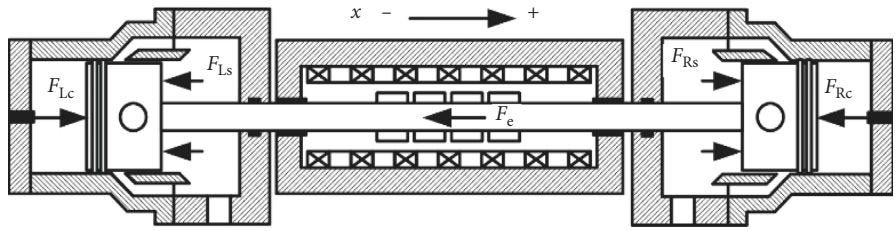

Figure 3: The prototype dynamics model.

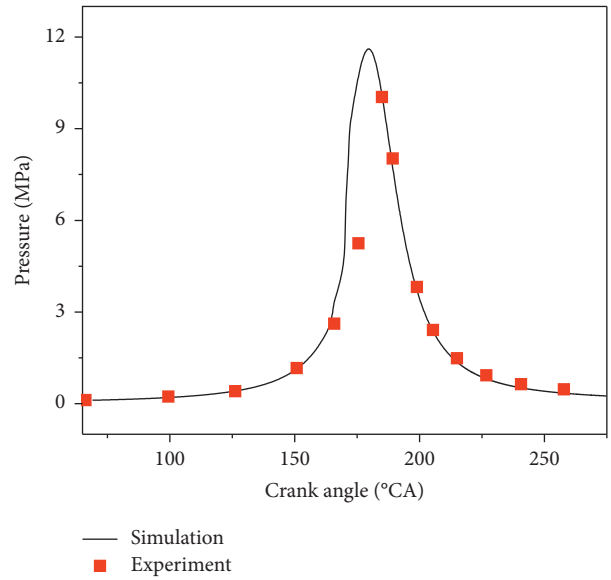

Figure 4: The simulation and experiment pressure curves.

Table 1: The in-cylinder distribution of C4H9OH concentration.

Butanol proportion	CA10	CA50	CA90
0	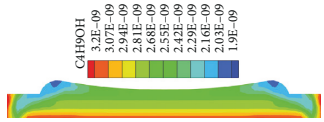	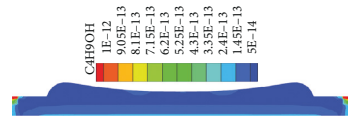	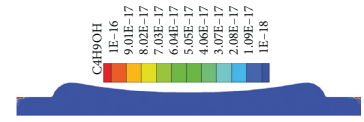
15%	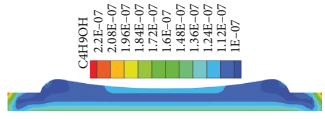	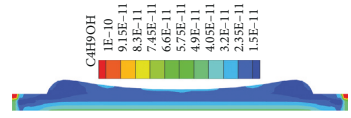	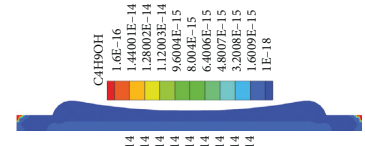
30%	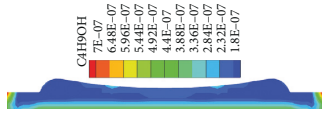	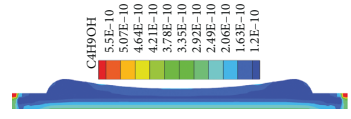	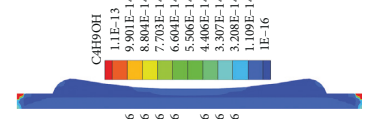
45%	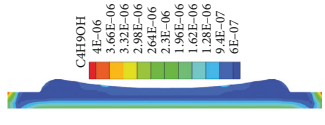	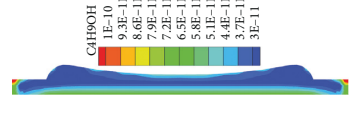	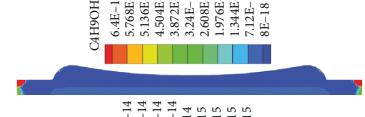
60%	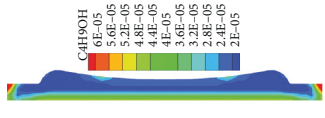	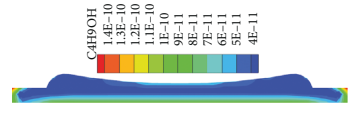	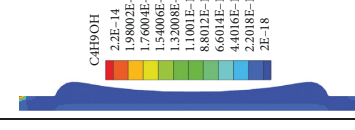

Table 2: The in-cylinder distribution of C7H16 concentration.

Butanol proportion	CA10	CA50	CA90
0	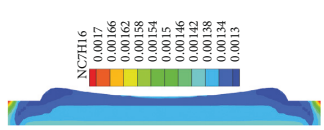	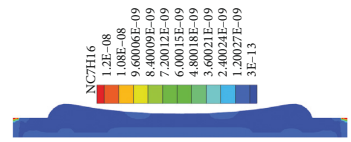	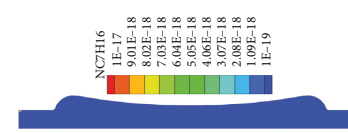
15%	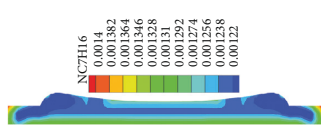	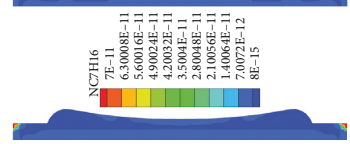	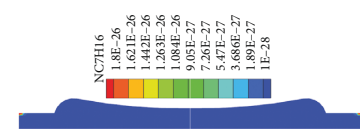
30%	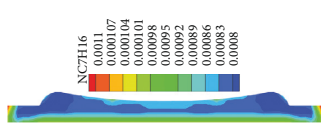	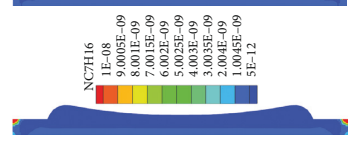	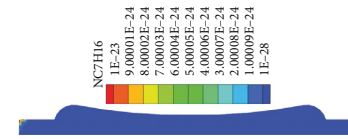
45%	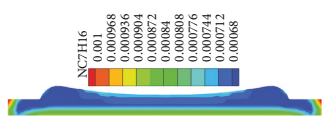	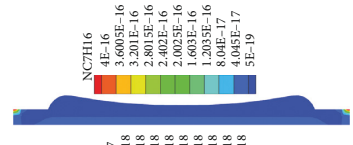	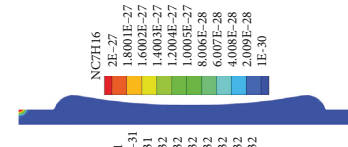
60%	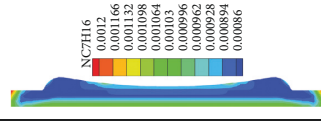	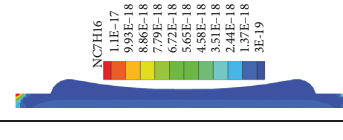	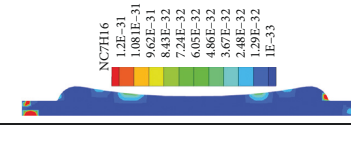

Table 3: The in-cylinder distribution of the nitric oxide concentration.

Butanol proportion	CA10	CA50	CA90
0	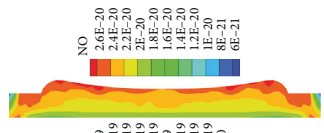	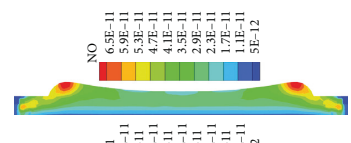	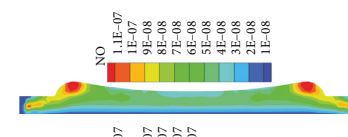
15%	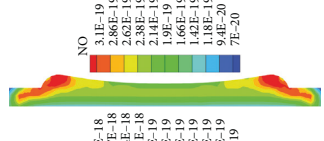	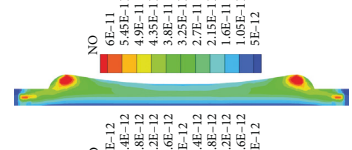	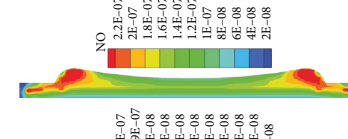
30%	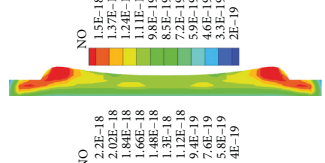	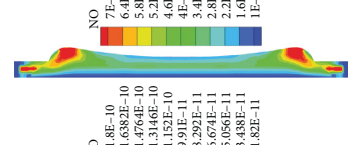	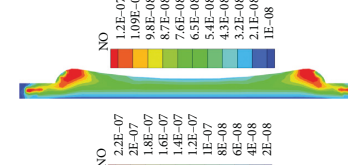
45%	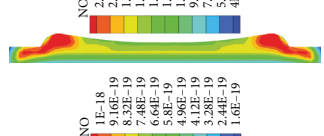	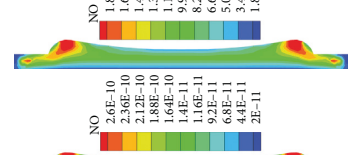	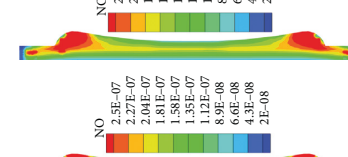
60%	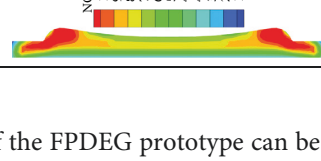	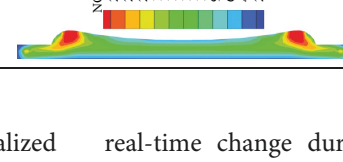	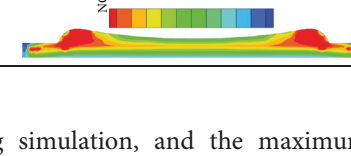

calculation process of the FPDEG prototype can be realized using the iterative calculation method shown in Figure 2, and the mesh generation of the prototype chamber was executed using the real-time grid processing technology [31]. In the process of importing the geometric model, the features of the geometric model were preserved precisely to generate the structured regular grid. When the grid density changed, the topology remained the same, which improved the calculation accuracy. The number of grids would have a real-time change during simulation, and the maximum number of grids was 1340888.

In addition, a detailed diesel fuel mechanism (*n*-heptane-*n*-butanol, 76 species) developed by Hu Wang's team [28] was integrated in the simulation model of the FPDEG prototype. Wang's mechanism had been validated on HCCI combustion with different volume fractions of *n*-heptane and *n*-butanol. The extended Zel'dovich NO_x mechanism was integrated in the emission model to calculate the NO_x

Table 4: The in-cylinder distribution of the carbon monoxide concentration.

Butanol proportion	CA10	CA50	CA90
0	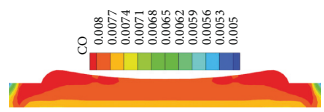	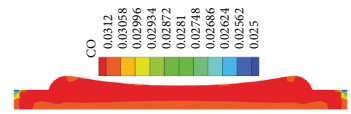	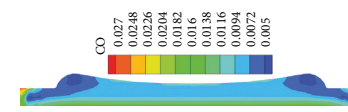
15%	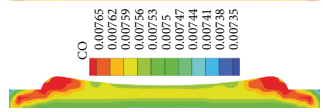	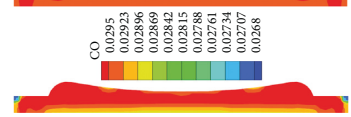	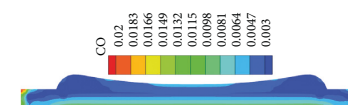
30%	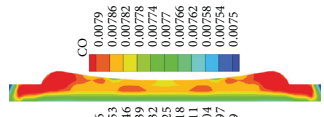	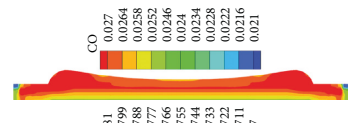	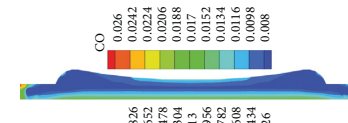
45%	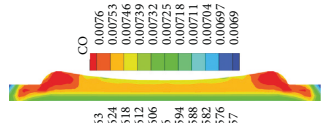	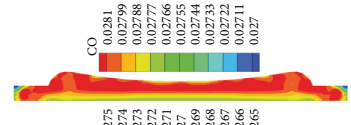	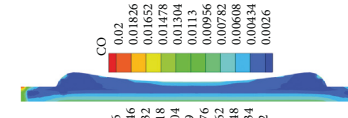
60%	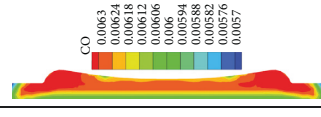	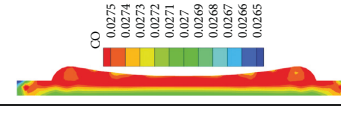	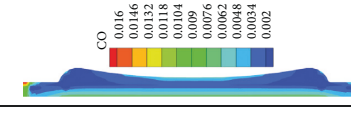

Table 5: The calculated temperature at different positions of the cylinder.

Butanol proportion	CAa10	CA50	CA90
0	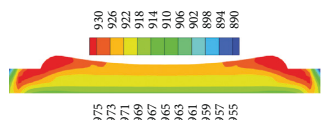	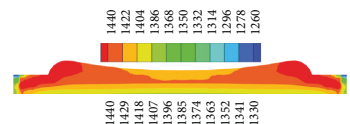	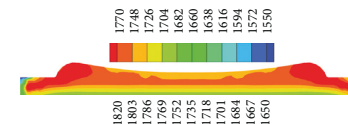
15%	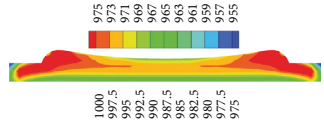	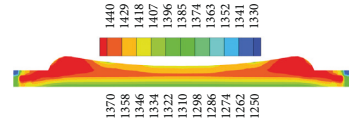	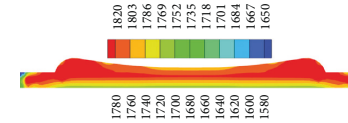
30%	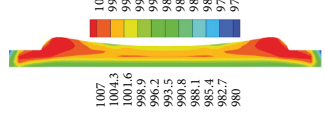	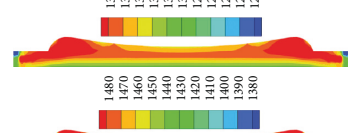	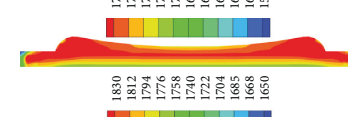
45%		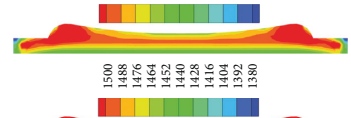	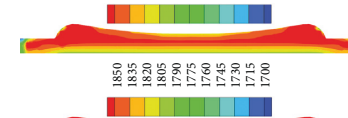
60%	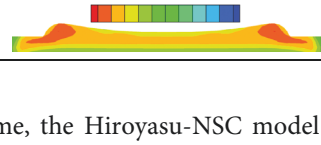	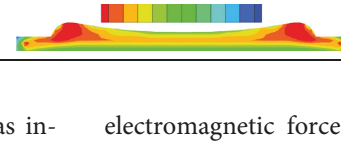	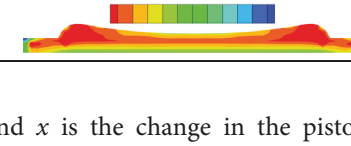

mass. In the meantime, the Hiroyasu-NSC model was introduced as a submodel of the emission model to calculate the total soot mass [32–35].

The prototype cylinder diameter was 60 mm. The free piston motion duration from was equivalent to 69°CA to 280°CA. The boundary conditions with the frictionless contact type were set as follows: the cylinder temperature was 450 K, the position temperature was 540 K, and the cylinder roughness was 0.5. Figure 3 shows the dynamics model of the prototype, and the equations of motion of the free piston can be expressed as follows:

$$m\frac{d^2x}{dt^2} = F_{Lc} - F_{Rc} - F_e - F_f. \quad (1)$$

In formula (1), m is the moving component mass, F_f is the friction of the system, F_{Lc} and F_{Rc} are the forces associated with gas on the left and right cylinder, F_e is the electromagnetic force, and x is the change in the piston position.

The thermodynamic model was established to solve for change in gas pressure in the FPDEG. The change rate of pressure p can be obtained by the following formula:

$$\frac{dp}{dt} = -\frac{\gamma p}{V}\frac{dV}{dt} + \frac{\gamma - 1}{V}\frac{dQ}{dt}. \quad (2)$$

In formula (2), Q is the energy of the FPDEG.

The initial conditions of the simulation were set to temperature $T_0 = 345$ K, pressure $P_0 = 1.14$ bar, and equivalent engine speed $n = 1374$ r/min. Figure 4 shows the simulation and experiment pure diesel fuel pressure curves [20]. It was seen that the simulation values of in-cylinder pressure near the top dead center were slightly higher than those of the experimental test results (the error is less than 5%). The reasons for the deviation are as follows: the setting of the

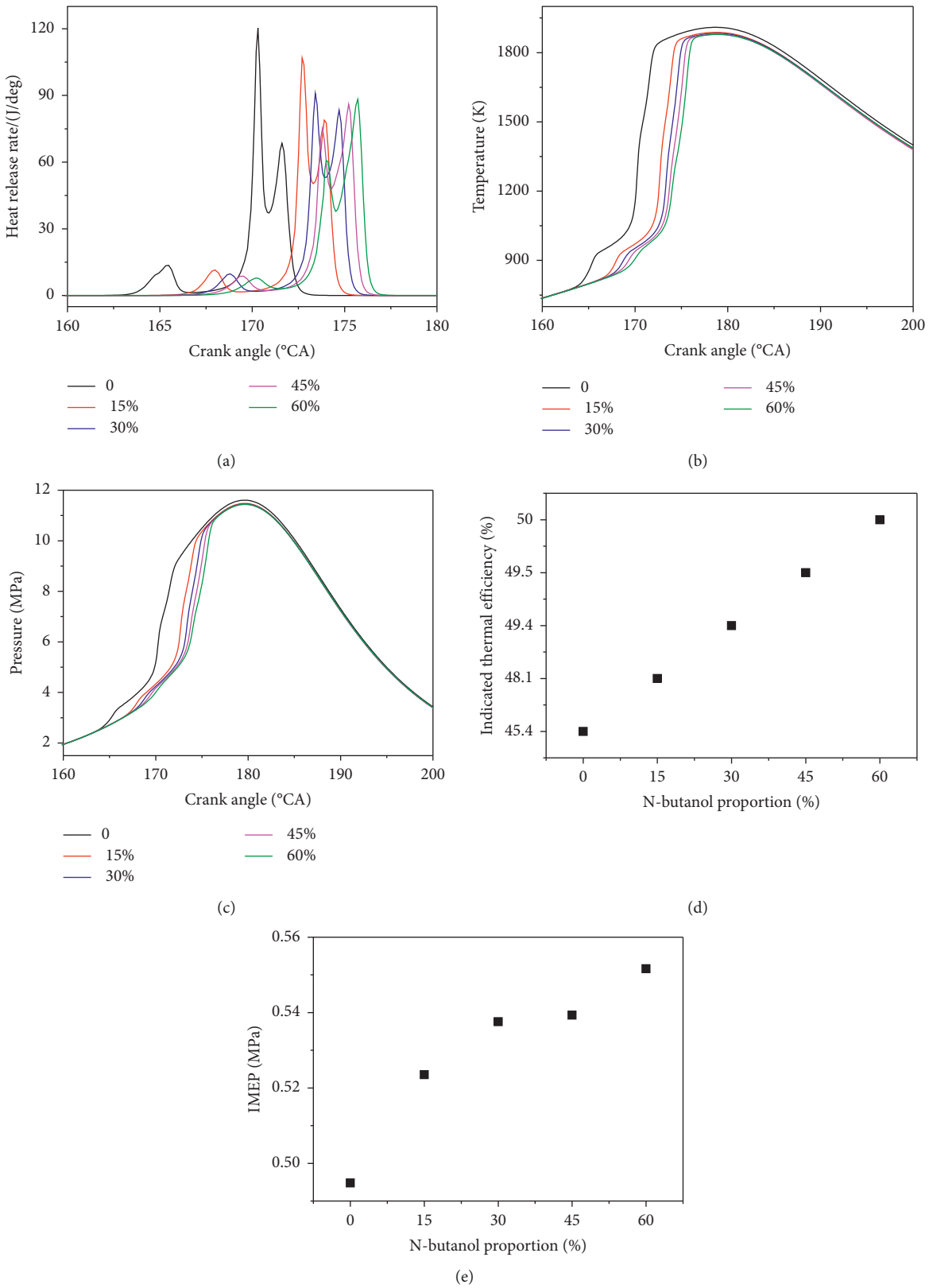

Figure 5: The combustion performance of different *n*-butanol proportions.

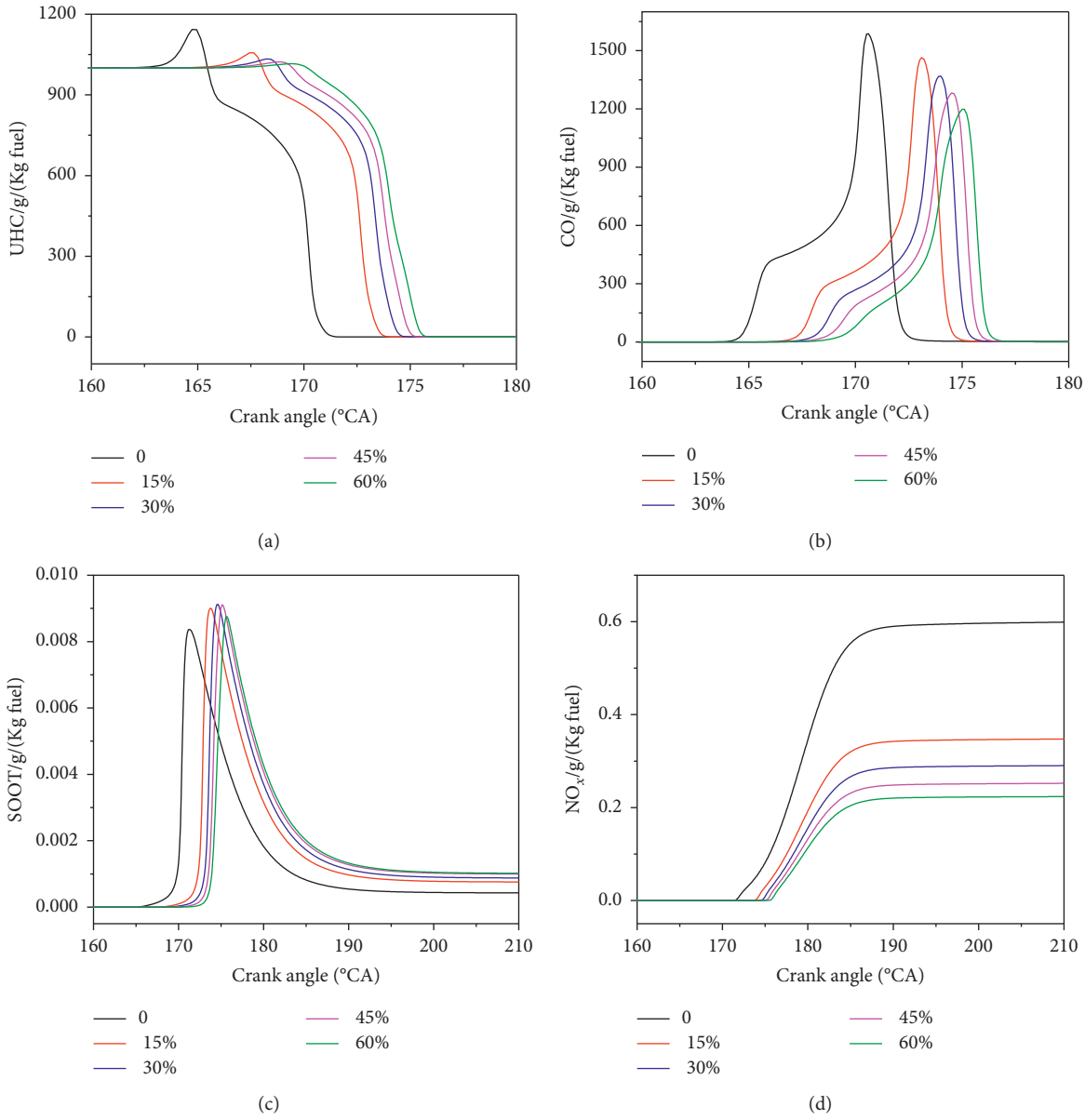

Figure 6: The emission performance of different *n*-butanol proportions.

initial condition deviates from the experimental state, the simulation is set to the adiabatic state, the calculation model has calculation error, and the test instrument has measurement error. Except the position near TDC, the simulation pressure curve was in good agreement with the experiment curve. The comparison of the pressure curves showed the validity of the simulation model that coupled the 76 species *n*-heptane-*n*-butanol mechanism. Therefore, the combustion performance of the FPDEG prototype can be obtained through this simulation model.

3. Simulation Results

3.1. The Effects of n-Butanol Proportion on Temperature and Species Concentration Distribution. In order to analyze the combustion process, three stages named CA10 (CA means the crank angle and 10 means 10% of the total heat release), CA50, and CA90 (same definition as CA10) were introduced. Tables 1 and 2 express the in-cylinder distribution of C4H9OH and C7H16 concentration, respectively. Tables 3 and 4 indicate the in-cylinder emission (nitric oxide and carbon monoxide) distribution, respectively. The calculated temperature at different positions of the cylinder is given in Table 5.

From Table 1 to Table 2, it can be seen that, at CA10, the C4H9OH and C7H16 were first oxidized near the two sides of the combustion chamber. At this moment, the concentration of the two species was uneven in the incipient space. Then, the C4H9OH and C7H16 were kept being oxidized until CA90. The final fuel concentration was very close to zero, and the fuel concentration distribution in the cylinder was quite uniform.

In Table 3, we can see that, at CA10, the NO was first produced near the two sides of the combustion chamber and

Table 6: The final content of UCH, soot, NO, and CO.

n-Butanol proportion	UCH	Soot	NO_x	CO
0	0.00586	4.38e-4	0.539	1.12
15%	0.00463	7.55e-4	0.312	0.723
30%	0.00545	8.74e-4	0.261	0.665
45%	0.00543	9.93e-4	0.227	0.574
60%	0.00653	0.001	0.2	0.55

the concentration distribution was extremely uneven in the cylinder. Then, the concentration kept increasing until CA90. The NO concentration reached its maximum at CA90, and the final NO concentration distribution in the cylinder was relatively uniform.

In Table 4, it can be seen that, at CA10, the CO was first produced near the two sides of the combustion chamber and the concentration distribution was extremely uneven in the cylinder. Then, the concentration kept increasing until CA50. After CA50, the CO would be oxidized to CO_2 until CA90. The final CO concentration was very close to zero, and the CO concentration distribution in the cylinder was quite uniform.

In Table 5, we can see that, at CA10, the temperature near the two sides of the combustion chamber was largest in the whole combustion chamber, and when the *n*-butanol proportion was 45%, the temperature on both sides of the combustion chamber was the highest. Then, from CA10 to CA90, the temperature rose rapidly and became more and more uniform in the cylinder.

3.2. The Effects of n-Butanol Proportion on Combustion Progress. Figure 5 shows the combustion performance curves of the different *n*-butanol proportions. It can be seen that, with 0%, 15%, 30%, 45%, and 60% of *n*-butanol, low-temperature combustion began at 162°CA, 165°CA, 165.6°CA, 166°CA, and 166.6°CA and the heat release rate was up to 13.6 J/deg, 11.5 J/deg, 9.7 J/deg, 8.6 J/deg, and 7.8 J/deg, which was mainly due to the later ignition delay of *n*-butanol. Corresponding to the five different proportions of *n*-butanol (0%, 15%, 30%, 45%, and 60%), high-temperature combustion began at 166.7°CA, 169.3°CA, 170.2°CA, 170.8°CA, and 171.4°CA and the heat release rate was up to 120.3 J/deg, 106.8 J/deg, 90.8 J/deg, 75.2 J/deg, and 60.7 J/deg. The highest point of the in-cylinder temperature curve and the corresponding proportion of *n*-butanol were 1909 K-0, 1888 K-15%, 1883 K-30%, 1880 K-45%, and 1879 K-60%, respectively. In the meantime, the highest points of the pressure curve and the corresponding proportion of *n*-butanol were 11.61 MPa-0, 11.48 MPa-15%, 11.46 MPa-30%, 11.44 MPa-45%, and 11.44 MPa-60%, respectively.

Apparently, the *n*-butanol proportion played a vital role in combustion progress. As the *n*-butanol proportion increased from 0 to 60%, the beginning crank angle of low-temperature combustion lagged by 4.6°CA and the beginning crank angle of high-temperature combustion lagged by 4.7°CA. Moreover, the maximum heat release rate decreased to 59.6 J/deg, and the highest points of the in-cylinder temperature and pressure curves decreased to 30 K and 0.17 MPa, respectively. Based on the above analysis, as the *n*-butanol proportion increased from 0 to 60%, the calculated indicated thermal efficiency augmented to 4.6% (from 45.4% to 50%) and the calculated indicated mean effective pressure increased to 0.057 MPa (from 0.495 to 0.552 MPa).

Figure 6 shows the emission performance curves of the different *n*-butanol proportions. It was seen that the increasing *n*-butanol proportion made the production of emissions lag by 4.3°CA, the final NO_x and CO content decrease to 0.239 and 0.57 g/kg fuel, respectively, and the final soot content increase to 0.000562 g/kg fuel.

The content (g/kg fuel) of the emissions is shown in Table 6.

4. Conclusions and Discussion

(1) By coupling the detailed fuel mechanism, the distribution of components and temperature in the cylinder can be obtained, which provides a basis for controlling the combustion process.

(2) The *n*-butanol proportion of diesel fuel played a vital role in combustion and emission progress of the FPDEG. As the *n*-butanol proportion increased from 0 to 60%, the beginning crank angle of low-temperature combustion and high-temperature combustion lagged by 4.6°CA and 4.7°CA, respectively. Moreover, the maximum heat release rate decreased to 59.6 J/deg, and the highest points of the in-cylinder temperature and pressure curves decreased to 30 K and 0.17 MPa, respectively. Furthermore, the calculated indicated thermal efficiency augmented to 4.6% (from 45.4% to 50%), and the calculated indicated mean effective pressure increased to 0.057 MPa.

(3) When HCCI combustion started (at CA10), the selected four species and temperature distributions were uneven. Through the entire combustion process (from CA10 to CA90), the final distributions of the selected four species and temperature were relatively uniform.

(4) With the increase in *n*-butanol proportion, the final NO_x and CO significantly diminished and the final soot content slightly increased. Therefore, the ratio of *n*-butanol should be appropriate to obtain the best emission.

Data Availability

The data used to support the findings of this study are available from the corresponding author upon request.

Conflicts of Interest

The authors declare that they have no conflicts of interest.

Acknowledgments

This work was supported by the Talent Introduction Project of Anhui Science and Technology University (grant number RCYJ201902), the University Synergy Innovation Program of Anhui Province (grant number GXXT-2019-020), and the College Students' Innovative Entrepreneurial Training Plan Program (grant number S202110879285).

References

[1] S. Onishi, J. S. Han, K. Shoda, J. P. Do, and S. Kato, "Active thermo-atmosphere combustion (ATAC): a new combustion process for internal combustion engine," *SAE Technical Paper*, vol. 88, Article ID 790501, 1979.

[2] M. Yao, Z. Zheng, and H. Liu, "Progress and recent trends in homogeneous charge compression ignition (HCCI) engines," *Progress in Energy and Combustion Science*, vol. 35, no. 5, pp. 398–437, 2009.

[3] H. Teng, H. D. Ng, K. Li, C. Luo, and Z. Jiang, "Evolution of cellular structures on oblique detonation surfaces," *Combustion and Flame*, vol. 162, no. 2, pp. 470–477, 2015.

[4] P. Yang, H. Teng, Z. Jiang, and H. D. Ng, "Effects of inflow Mach number on oblique detonation initiation with a two-step induction-reaction kinetic model," *Combustion and Flame*, vol. 193, pp. 246–256, 2018.

[5] K. Epping, S. Aceves, R. Bechtold, and J. Dec, *The Potential of HCCI Combustion for High Efficiency and Low Emissions*, SAE, Warrendale, PA, USA, 2002.

[6] S. L. Kokjohn, R. M. Hanson, D. A. Splitter, and R. D. Reitz, "Experiments and modeling of dual-fuel HCCI and PCCI combustion using in-cylinder fuel blending," *SAE International Journal of Engines*, vol. 2, no. 2, pp. 24–39, 2010.

[7] S. Tanaka, F. Ayala, J. C. Keck, and J. B. Heywood, "Two-stage ignition in HCCI combustion and HCCI control by fuels and additives," *Combustion and Flame*, vol. 132, no. 1, pp. 219–239, 2003.

[8] G. M. Shaver, J. C. Gerdes, M. J. Roelle, P. A. Caton, and C. F. Edwards, "Dynamic modeling of residual-affected homogeneous charge compression ignition engines with variable valve actuation," *Journal of Dynamic Systems, Measurement, and Control*, vol. 127, no. 3, pp. 374–381, 2005.

[9] G. M. Shaver, J. C. Gerdes, and M. J. Roelle, "Physics-based modeling and control of residual-affected HCCI engines," *Journal of Dynamic Systems, Measurement, and Control*, vol. 131, no. 2, Article ID 021002, 2009.

[10] Y. Xu, H. Zhang, F. Yang et al., "Experimental investigation of pneumatic motor for transport application," *Renewable Energy*, vol. 179, pp. 517–527, 2021.

[11] D. Cui, H. Yin, Y. Liu, J. Li, S. Pan, and Q. Wang, "Effect of final pyrolysis temperature on the composition and structure of shale oil: synergistic use of multiple analysis and testing methods," *Energy*, vol. 252, Article ID 124062, 2022.

[12] C. Zhang, K. Li, and Z. Sun, "Modeling of piston trajectory-based HCCI combustion enabled by a free piston engine," *Applied Energy*, vol. 139, pp. 313–326, 2015.

[13] R. Mikalsen and A. P. Roskilly, "A review of free-piston engine history and applications," *Applied Thermal Engineering*, vol. 27, no. 14, pp. 2339–2352, 2007.

[14] Y. Wu, Y. Wang, X. Zhen, S. Guan, and J. Wang, "Three-dimensional CFD (computational fluid dynamics) analysis of scavenging process in a two-stroke free-piston engine," *Energy*, vol. 68, pp. 167–173, 2014.

[15] B. Jia, Z. Zuo, G. Tian, H. Feng, and A. P. Roskilly, "Development and validation of a free-piston engine generator numerical model," *Energy Conversion and Management*, vol. 91, pp. 333–341, 2015.

[16] C. M. Atkinson, S. Petreanu, N. N. Clark et al., *Numerical Simulation of a Two-Stroke Linear Engine*, SAE Paper, Warrendale, PA, USA, 1999.

[17] W. R. Cawthorne, P. Famouri, J. D. Jingdong Chen et al., "Development of a linear alternator-engine for hybrid electric vehicle applications," *IEEE Transactions on Vehicular Technology*, vol. 48, no. 6, pp. 1797–1802, 1999.

[18] S. Plsek, P. Deutsch, and O. Vysoky, "In-cycle thermodynamic model of linear combustion engine," in *Proceedings of the IEEE Conference on Computer Aided Control System Design*, IEEE, Munich, Germany, October 2006.

[19] Q. Li, J. Xiao, and Z. Huang, "Simulation of a two-stroke free-piston engine for electrical power generation," *Energy and Fuels*, vol. 22, no. 5, pp. 3443–3449, 2008.

[20] H. Feng, C. Guo, C. Yuan et al., "Research on combustion process of a free piston diesel linear generator," *Applied Energy*, vol. 161, pp. 395–403, 2016.

[21] C. Yuan, H. Feng, Y. He, and J. Xu, "Combustion characteristics analysis of a free-piston engine generator coupling with dynamic and scavenging," *Energy*, vol. 102, pp. 637–649, 2016.

[22] R. Mikalsen and A. P. Roskilly, "Coupled dynamic-multidimensional modelling of free-piston engine combustion," *Applied Energy*, vol. 86, no. 1, pp. 89–95, 2009.

[23] R. Mikalsen and A. P. Roskilly, "A computational study of free-piston diesel engine combustion," *Applied Energy*, vol. 86, no. 7-8, pp. 1136–1143, 2009.

[24] M. Bergman, J. Fredriksson, and V. Golovitchev, "CFD-base optimization of a diesel-fueled free piston engine prototype for conventional and HCCI combustion," *SAE International Journal of Engines*, vol. 1, no. 1, pp. 1118–1143, 2009.

[25] S. Ren, B. Ye, S. Li, L. Pang, Y. Pan, and H. Tang, "Well-defined coordination environment breaks the bottleneck of organic synthesis: single-atom palladium catalyzed hydrosilylation of internal alkynes," *Nano Research*, vol. 15, no. 2, pp. 1500–1508, 2021.

[26] J.-S. Jia, Y. Cao, T.-X. Wu et al., "Highly regio- and stereoselective markovnikov hydrosilylation of alkynes catalyzed by high-nuclearity {Co14} clusters," *ACS Catalysis*, vol. 11, no. 12, pp. 6944–6950, 2021.

[27] Z. Cheng, Z. Guo, P. Fu, J. Yang, and Q. Wang, "New insights into the effects of methane and oxygen on heat/mass transfer in reactive porous media," *International Communications in Heat and Mass Transfer*, vol. 129, Article ID 105652, 2021.

[28] H. Wang, R. D. Reitz, M. Yao, B. Yang, Q. Jiao, and L. Qiu, "Development of an n-heptane-n-butanol-PAH mechanism and its application for combustion and soot prediction," *Combustion and Flame*, vol. 160, pp. 504–519, 2013.

[29] C. Liu and K. Yi, "Integrated reduction of large chemical kinetic model of bio-butanol," *Desalination and Water Treatment*, vol. 219, pp. 172–177, 2021.

[30] H. Feng, Y. Song, Z. Zuo, J. Shang, Y. Wang, and A. P. Roskilly, "Stable operation and electricity generating characteristics of a single-cylinder free piston engine linear generator: simulation and experiments," *Energies*, vol. 8, no. 2, pp. 765–785, 2015.

[31] C. H. Liu, S. J. Wu, and S. Pang, "Effects of five different parameters on biodiesel HCCI combustion in free-piston engine generator," *Thermal Science*, vol. 25, no. 6, pp. 4197–4207, 2021.

[32] Y. Peng, Z. Xu, M. Wang et al., "Investigation of frequency-up conversion effect on the performance improvement of stack-based piezoelectric generators," *Renewable Energy*, vol. 172, pp. 551–563, 2021.

[33] R. J. Zhang, W. Zhang, J. D. Dong, L. N. Ma, Z. X. Jiang, and Y. D. Huang, "3d hierarchical oxygen-deficient alconi-(Oxy) hydroxides/N-doped carbon hybrids enable efficient battery-type asymmetric supercapacitor," 2022, https://ssrn.com/abstract=4017632%20or%20http://dx.doi.org/10.2139/ssrn.4017632.

[34] H. Liu, Y. Wang, Q. Li, N. Yang, Z. Wang, and Q. Wang, "Research on the evolution characteristics of oxygen-containing functional groups during the combustion process of the torrefied corn stalk," *Biomass and Bioenergy*, vol. 158, Article ID 106343, 2022.

[35] H. Hiroyasu, T. Kadota, and M. Arai, "Development and use of a spray combustion modeling to predict diesel engine efficiency and pollutant emissions: Part 1 combustion modeling," *Bulletin of JSME*, vol. 26, no. 214, pp. 569–575, 1983.